Aeroelastic Analysis of Nonlinear High Aspect Ratio Wings

Christian Spada

Instituto Superior Técnico, Universidade de Lisboa, Lisboa, Portugal, October 2014

Abstract: Nowadays the aeronautic industry struggles with the demand to enhance flight efficiency and to reduce emissions at the same time. One solution for reducing fuel consumption is increasing wing aspect ratio since it improves the lift-to-drag ratio. Nevertheless, higher deflections are expected, which may lead to relevant nonlinear aeroelastic behavior. In this work, a reference regional aircraft wing structural layout is designed to ensure structural integrity for a load limit of 3.8 g's. A scaled model that represents well the aeroelastic behavior is required for wind tunnel testing to evaluate the nonlinear behavior that can occur in high aspect ratio wings. For this purpose, two classical scaling methodologies were employed. These methodologies use scaling factors that are derived from the governing aeroelastic equations of motion. The first does a direct modal response matching, while the second uncouples the mass and stiffness distribution to achieve the modal response. The scaled structure design parameters are optimized to obtain the target scaled values. The methodologies are compared and the achieved configuration that better represents the full model behavior is selected. A new nonlinear aeroelastic scaling methodology using Equivalent Static Loads was developed, which uses two different optimization routines to match the nonlinear static response and the mode shapes of the full model. Results show marked improvement when applying this approach to design the scaled model.

1. Introduction

In recent years, the trend is to design aircraft with high aspect ratio wings, especially for civil and commercial aircraft. This trend occurs because this configuration offers great advantages. In general this setup produces more lift and provide aircraft with a higher lift-to-drag ratio and endurance flight [1]. To make the concept feasible in terms of weight restrictions, these wings are very flexible. High aspect ratio wings increase efficiency because they produce less induced drag leading to lower fuel consumptions. The total drag coefficient can be defined as:

$$C_D = C_{D0} + C_{Di} = C_{D0} + \frac{C_L^2}{\pi \cdot e' \cdot AR}$$

Equation 1.1: Total drag coefficient

where:

C_{D0} Profile drag coefficient

C_{Di} Induced drag coefficient

C_L Lift coefficient

e' Span efficiency factor, which is unity if the wing planform is elliptical

AR Aspect ratio

Note that the induced drag, which is mainly due to the presence of the wing tip trailing vortex, can be decreased by increasing the aspect ratio.

Nevertheless this challenge requires detailed studies due to large deformations under normal operating loads leading to a geometrical nonlinear behavior and aeroelastic problems [5]. These large deformations can change the natural frequencies of the wing which can produce noticeable changes in its aeroelastic behavior [4].

In order to better understand the physical behavior of the wing without building an expensive

full scale demonstrator, a reduced scale model must be designed.

Aeroelastic scaling requires consideration of aerodynamic and structural physics. Aerodynamic similitude is achieved analytically. Flight conditions such as airspeed and altitude are selected for matching scaled parameters like Froude number and density ratio, for example. Structural similitude is not realistically achievable by geometrically scaling the structural components. Corresponding analytical scaling requirements will generally specify that a geometrically scaled structure should be made from materials that have unobtainable properties. There is also a high probability that the manufacturing techniques used for the full scale design cannot be duplicated at a smaller scale. The only feasible option is to redesign the internal structure and optimize it such that its scaled mass and stiffness properties are consistent with the full scale aircraft [11]. The ladder structure is one of several scaled model configurations recommended by Bisplinghoff *et al.* [3].

In the classical approach, aeroelastic scaling is achieved by selection of a discrete subset and modal degrees of freedom that capture the relevant global properties of the full model, and optimizing the scaled aircraft such that the nondimensional modal masses and stiffness coefficients match the full scale aircraft.

The most common practice for classical aeroelastic scaling is to use a truncated number of the vibration mode shapes from the target full scale model as the modal degrees of freedom for the scaled model optimization [2, 12]. There is although a drawback, the truncation may omit information that becomes important when geometric nonlinearities are significant (it can be considered analogous to not modeling certain flexibilities (e.g., axial and shear)). Classical scaling methods have worked in practice for traditional applications, but the validity of the modeling assumptions needs verification for cases where geometric nonlinearities are important.

2. Theory

Due to the fact of the complex nature of the problem, a simplified physics model was chosen: the small disturbance, linear potential partial differential equations (PDE) [13]. This model reduces the degrees of freedom into only two: displacement and rotation;

$$\begin{bmatrix} M_{11} & M_{12} \\ M_{21} & M_{22} \end{bmatrix} \begin{Bmatrix} \ddot{X} \\ \ddot{\theta} \end{Bmatrix} + \begin{bmatrix} K_{11} & K_{12} \\ K_{21} & K_{22} \end{bmatrix} \begin{Bmatrix} X \\ \theta \end{Bmatrix} = \frac{\rho \cdot V^2}{2} \begin{bmatrix} b^2 & 0 \\ 0 & b^3 \end{bmatrix} \begin{bmatrix} Q_{11} & Q_{12} \\ Q_{21} & Q_{22} \end{bmatrix} \begin{Bmatrix} X \\ \theta \end{Bmatrix}$$

Equation 2.1: Small Disturbance, Linear Potential Partial Difference Equations (PDE)

where:

X	Vector of translational degrees of freedom
θ	Vector of rotational degrees of freedom
M_{ij}	Block matrix terms in inertia/mass matrix
K_{ij}	Block matrix terms in stiffness matrix
b	Reference length
Q_{ij}	Block matrix of aerodynamic terms

Even though these physics are limited, the PDE equations are adequate for a low-cost exploration of flight mechanics in real world conditions. In this work it is only analyzed the free vibration case, so the right part of the *Equation 2.1* disappear and the system of equations become (see *Equation 2.2*):

$$\begin{bmatrix} M_{11} & M_{12} \\ M_{21} & M_{22} \end{bmatrix} \begin{Bmatrix} \ddot{X} \\ \ddot{\theta} \end{Bmatrix} + \begin{bmatrix} K_{11} & K_{12} \\ K_{21} & K_{22} \end{bmatrix} \begin{Bmatrix} X \\ \theta \end{Bmatrix} = \begin{Bmatrix} 0 \\ 0 \end{Bmatrix}$$

Equation 2.2: Free-vibrations System of Equations

2.1 Scaling Factors

The geometrically scaled model is constrained by a set of scaling parameters. These scaling factors are

derived from non-dimensional parameters, which appear in the equations that govern the aerodynamics, the structure and their coupling. The choice of these scaling parameters is subject to constraints posed by the wind tunnel or environment in which the model will operate.

For the purpose of obtaining a non-dimensional set of equations the designer has to choose three primary quantities, which are the only parameters that can be changed. There is a great range of choices that could be made, however only one combination is investigated here which is the combination selected for this work [2]:

- the span *b* (based on the desired reduced scale span, it is due to wind tunnel constraints);
- air density *ρ* (it is due to environmental constraints);
- velocity *V* (it is due to wind tunnel constraints).

These are the primary quantities used in the Buckingham π theorem that is applied to the other important properties, which are needed for a good aeroelastic similitude between full scale and reduced size models. The factors used to attain to the aeroelastic scaling are summarized in *Table 2.1*.

SCALING FACTORS			
Length Scale	$n_g = \frac{b_s}{b_f}$	**Mass Ratio**	$n_M = \frac{M_s}{M_f} = n_g^3 \cdot n_\rho$
Air Density ratio	$n_\rho = \frac{\rho_s}{\rho_f}$	**Frequency Ratio**	$n_f = \frac{f_s}{f_f} = \frac{n_v}{n_g}$
Velocity Ratio	$n_v = \frac{V_s}{V_f}$	**Force Ratio**	$n_F = \frac{F_s}{F_f} = n_\rho \cdot n_v^2 \cdot n_g^2$

Table 2.1: Scaling Factors, the subscripts of *s* and *f* represent scaled and full scale respectively.

The Froude number is a ratio between inertial and gravitational forces and in turn determines the ratio of deflections due to gravity compared to those due to aerodynamic forces. In many cases, the deflection due to gravity can be assumed insignificant compared to aerodynamic forces. If this assumption is valid the Froude number can be ignored (often the case in wind tunnel). However, in the case of the unconstrained model in free flight, the Froude number may play a more significant role [13]. In order to maintain a similitude of Froude number, the following ratio (see *Equation 2.3*) must be maintained:

$$\left(\frac{V}{\sqrt{b \cdot g}}\right)_s = \left(\frac{V}{\sqrt{b \cdot g}}\right)_f$$

Equation 2.3: Froude number

The task of matching the Reynolds number at a desired velocity-altitude is a difficult one. It requires that the viscosity of the surrounding medium be changed, which in most cases is not easily accomplished. For this reason the matching of the Reynolds number will likely not be satisfied. Although this may seem of concern, experience has shown that it is generally of minor importance as far as aeroelastic effects for main lifting surfaces are concerned [10].

The scaling based on simplified physic model permit a reduction of the model restrictions, which would be much more complex if it was chosen a scaling based on the Navier-Stokes equations.

2.2 Scaling Methodologies - Classical Approach

One design approach for developing accurate mass and stiffness distribution is to scale down the exact geometry of the full scale model.

Unfortunately, this is not practical for several reasons. For instance, the manufacture of scaled components may be very expensive and in some cases impossible due to their small resulting sizes.

There is the need to find an alternative to the exact scaling of the full scale model geometry in order to achieve a match between the two models mass and stiffness distributions while at the same time ensuring manufacturability [12]. From the governing equations of linear elasticity, it can be proved that every model, which has the same scaled geometry and the same scaled mass and stiffness distributions, will result in the same modal response (mode shapes and frequencies) as those of the full model, after appropriate scaling [9]. From the full scale model are obtained the target values that should be attained by the scaled models. To achieve the target values two different classical scaling methodologies can be used.

The first match the modal response directly (Method 1) while the second one match the modal response through a mass and stiffness distributions uncoupling (Method 2). In *Figures 2.1a* and *2.1b* are shown the Method 1 and the Method 2 diagram respectively. For more details it is advisable to consult reference [14].

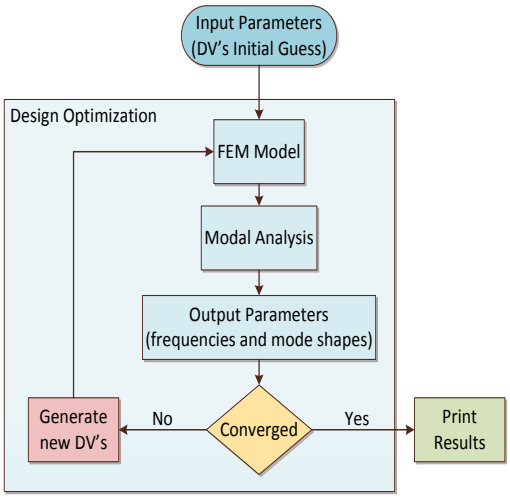

(a): Method 1

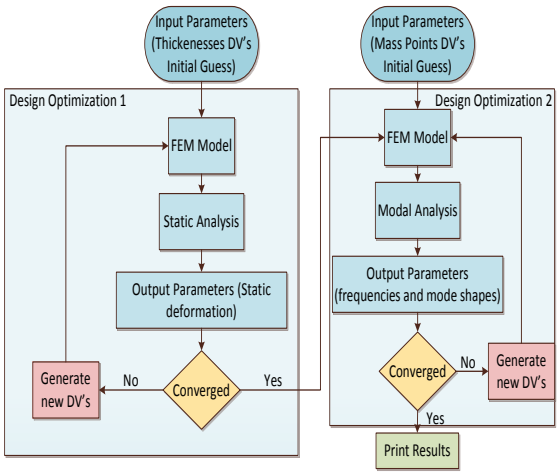

(b): Method 2

Figure 2.1: Scaling Methodologies

2.3 Scaling Methodologies - Modern Approach

Direct optimization of the nonlinear static response is a computationally intensive task. Efficiency can be gained by transformation to an equivalent linear system using the equivalent static loads approach [8]. The *ESL* is defined as the static load that generates the same displacement field by an analysis which is not linear static and it requires an iterative procedure that updates the linearized system as the design changes. The basic idea of *ESL* is presented in *Figure 2.2*.

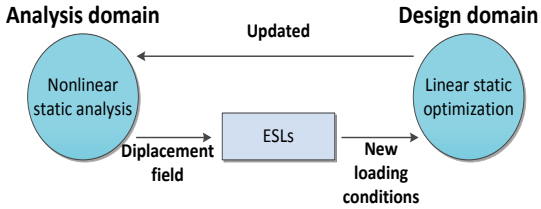

Figure 2.2: Schematic process between the analysis and the design domain respectively

The optimization process is divided into two domains: analysis and design domain respectively.

Nonlinear static analysis is performed in the analysis domain. The nonlinear displacement field is evaluated and the equivalent load sets are evaluated in order to ensure the same displacement field between nonlinear and linear

static analysis. The equivalent load sets are transferred to the design domain. In the design domain, linear static optimization is performed by using the equivalent loads as external loads. The design variables are updated in the design domain and nonlinear static analysis is performed again with the update design variables. The process proceeds until the convergence criteria is satisfied. The new scaling methodology including geometric nonlinearities is shown in *Figure 2.3*. For more details it is advisable to consult reference [14].

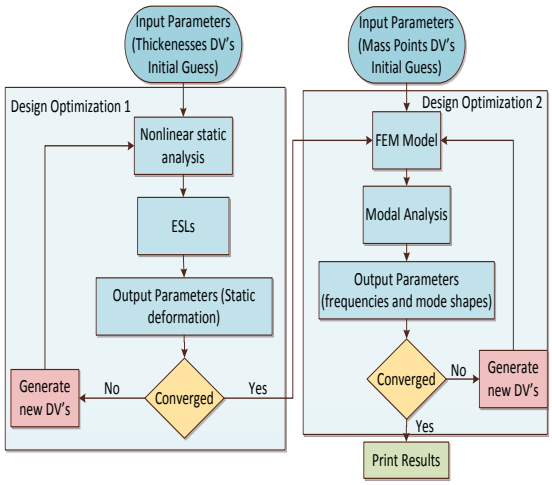

Figure 2.3: Scaling methodology including geometric nonlinearities

3. Full Model

The wing is based on the NOVEMOR project of the EU 7th framework reference wing, which was altered to exhibit a higher aspect ratio of twelve. On the baseline model the wing contains an industrial standard two-spar configuration at 25% and 75% chord. In order to keep the internal configuration of the wing simple and to avoid further problems on the scaling of the full model, the pylon and the wing are modeled with equally spaced ribs. In the section where the engine is placed it was decided to add another rib with the purpose of increasing the wing stiffness. Figure 3.1 shows the external and internal structural wing model used in the calculations. The software used was *MSC Nastran*™. For geometric details consult reference [14].

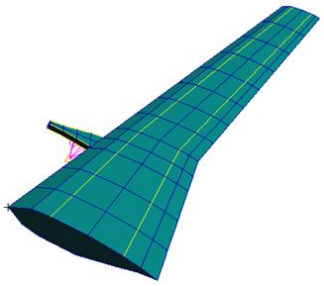

(a): External configuration of the wing

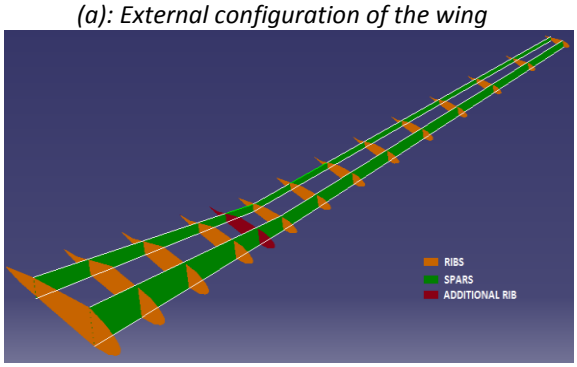

(b): Internal configuration of the wing

Figure 3.1: Structural Model

The structural layout is designed to ensure structural integrity for a load limit of 3.8 g's. Linear and nonlinear static analyses are performed in order to evaluate the differences between the two analyses. For all the components of the structural model the material selected is the *7075 Aluminum* alloy.

Important differences between linear and nonlinear results are observed. *Figure 3.2a* shows the differences in terms of tip deflection when linear and nonlinear static analyses are performed for different values of load factor. The results diverge gradually increasing the load factor. At 4g, tip deflection is about 2.4 times lower what is predicted by linear analysis. *Figure 3.2b* and *3.2c* shows the variation of the bending and twist angle respectively belong the wing span for a load factor equal to one when the two analyses are performed. The results confirm that the structure experiences a stiffness hardening effect when a nonlinear static analysis is performed.

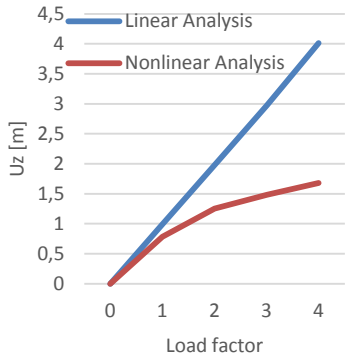

(a):Variation of the tip deflection

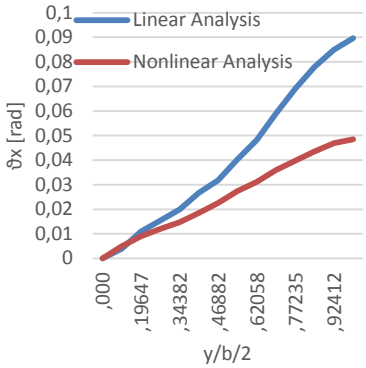

(b): Variation of the bending angle

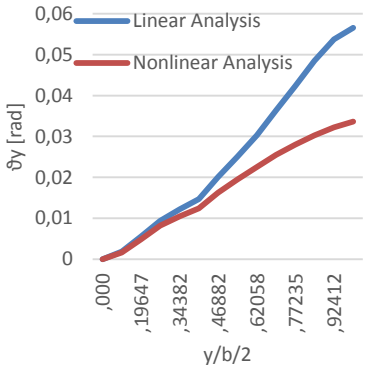

(c): Variation of the twist angle

Figure 3.2: Variation of the tip deflection, bending and twist angle along the wing span (n_z=1) in condition of empty tanks when linear and nonlinear analyses are performed

4. Scaled Model

The present document is a resume of the thesis [14]. Only the best configuration, i.e. *Configuration 2*, is treated in this paper. In this *Configuration* the wing is scaled as a ladder structure. Rectangular spars placed at 25% and 75% chord and cylindrical rungs are tailored to match the required stiffness. Beam elements are most appropriate to model this ladder structure. In order to maintain the aerodynamic shape of the airfoil, it was decided to model the wing skins with shell elements to simulate the behavior of a very thin layer (0.5 millimeters) of *Balsa* material. *Balsa* ribs would provide local support.

The pylon is an exact scale down of the full scale model and in accordance with the reference [7] it is modeled by beam and shell elements in order to model the caps and webs respectively.

In order to properly represent the full model by the scaled model, it was decided to match the first seven natural frequencies and respective translational and rotational modes with a discrepancy of 5%. This choice is due because the flutter phenomenon occurs as result of coupling of the bending (fourth mode) and torsional (seventh mode) natural modes of the wing. Also the overall mass should not exceed the 5% of error margin.

The geometry of the scaled model is externally the exact geometric scale of the full scale model. A question is to find the best material to model the structural components of the scaled structure. An exact scale of the *7075 Aluminum* alloy will lead to a none existing isotropic material. Three materials (*7075 Aluminum*, *Elektron 43* and *Stainless Steel*) were chosen for a comparison study, and from which the *Elektron 43* was the one that presented the lowest average error (162%) in comparison with the target scaled material, so it was selected to be scaled model material. The design variables are the following parameters: width and height of the front and rear wing spars, diameter of wing rungs, size of the front and rear pylon spars, thickness of the ribs of the pylon and lumped masses, for the state variables all the

properties to be match (mass, natural frequencies, mode shapes and in Method 2 also the static deflection makes part), which also take part of the Objective function to minimize. Sum of the squares of the residuals (SSR) is the most basic scheme for quantifying differences in the responses.

5. Classical Approach

In this section the comparison between Method 1 (see *Figure 2.1a*) and Method 2 (see *Figure 2.1b*) is made only for the best configuration studied, i.e. *Configuration 2*. *Table 5.1* summarizes the most relevant results for both methods.

	Method 1	Method 2
Global average error	4.49 %	4.70%
Computational Time	29.1 *h*	17.4 h (7 *h* + 10.4 *h*)
Number of DV's	86	86 (50 +36)

Table 5.1: Result comparison for Configuration 2

From *Table 5.1* it is observable that Method 1 allows obtaining a global average error slightly lower compared to Method 2, but the latter considerably needs less computational time to attain good results. Global average error is obtained as an average of the errors (natural frequencies, overall mass) and average errors (translational and rotational mode shapes, in Method 2 the static deflection is also included).

The difference between the global average errors of both methods is not high, 0.21%. *Figure 5.1* shows the differences between Method 1 and Method 2 in order to match the first seven natural frequencies and respective mode shapes of the full model. The ordinate of the plots is normalized with the relative target value in order to improve the interpretation of results (for example in *Figure 5.1a* the ordinate of the plot is equal to $\frac{f^T - error \cdot f^T}{f^T}$).

From *Figure 5.1* one can note that Method 1 is the most accurate especially if it is necessary to match the natural frequencies and respective mode shapes over the second mode. The first natural frequencies and respective mode shapes are pretty simple to check, the last are more complicated for both methods. However, the differences between the two methods are not very high.

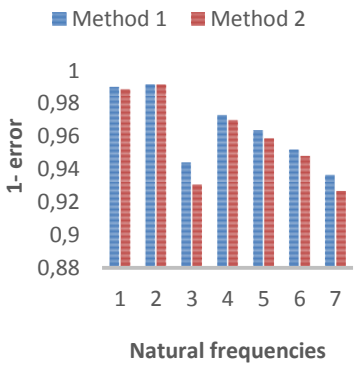

(a): Natural frequencies

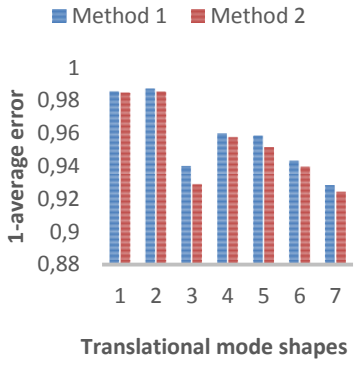

(b): Translational mode shapes

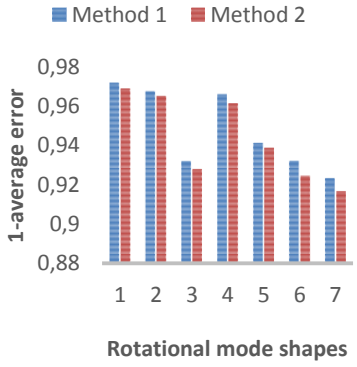

(c): Rotational mode shapes

Figure 5.1: Discrepancies between the two Methods in order to match the first seven natural frequencies, translational and rotational mode shapes of the full model

From the employed scaling methodologies, it is recommended to use Method 2, due to the lower computational time required to attain good results, which can be of great relevancy. The mode shapes images can be consulted in reference [14]. The optimization process has not been able to obtain errors and average errors less than 5%.

6. Modern Approach

The purpose of this section is to compare the results between the optimized scaled design obtained in Section 5 with the same structural model obtained by applying the methodology represented in *Figure 2.3*. The design optimization converges in seven nonlinear iterations and the final results are summarized in *Table 6.1*.

	Classical Approach (Method 2)	Modern Approach (ESL)
Global average error	4.70 %	4.01%
Computational Time	17.4 h (7 *h* + 10.4 *h*)	55 h (47 *h* + 8 *h*)
Number of DV's	86	

Table 6.1: Results comparison between classical and modern approach

From *Table 6.1* it is observable that the modern approach (ESL) allows obtaining a global average error lower compared to classical approach (Method 2), but the latter considerably needs less computational time to attain good results. Therefore, the modern approach is not recommended when the structure does not experience nonlinear effects. The main improvement concerns the matching of the mass, the translation of the fourth mode shape (see *Figure 6.1b*) and the rotations of the sixth and seventh mode shape (see *Figure 6.1c*). The size of the design parameters in the modern approach are lower than the classical approach and this is the main reason because the overall mass error in modern approach (2.34%) is lower than the classical approach (5.71%).

Figure 6.1 shows the differences between the classical (Method 2) and modern (*ESL*) approach in order to match the first seven natural frequencies and respective mode shapes of the full model. The ordinate of the plots is again normalized with the relative target value in order to improve the interpretation of results (see Section 5). The same computer was used. However the optimization process has not been able also in the modern approach to obtain errors and average errors less than 5% and this is mainly due to the complexity of the structural model. The mode shapes images can be consulted in reference [14].

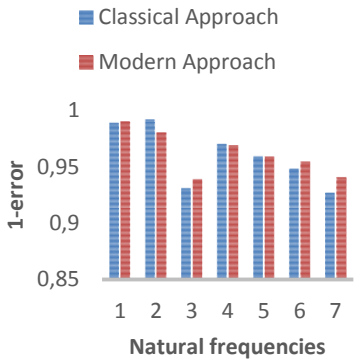

(a): Natural frequencies

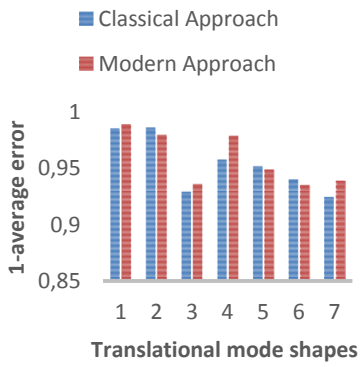

(b): Translational mode shapes

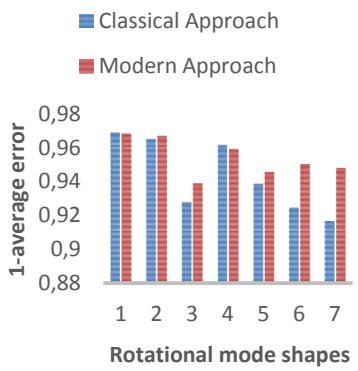

(c): Rotational mode shapes

Figure 6.1: Discrepancies between the two Methods in order to match the first seven natural frequencies, translational and rotational mode shapes of the full model

7. Conclusions and Future Work

Classical and modern approaches to aeroelastic scaling were reviewed. Truncation of higher-frequency modal degrees of freedom from the classical scaling optimization may lead to designs that do not correctly capture the nonlinear kinematic effects. Two methods, Method 1 and Method 2, have been developed that describe the classical approach for aeroelastic scaling. From the scaling methodologies applied, it is recommended the employment of Method 2, due to the lower computational time required to attain good results, which can be of great relevancy.

A modern aeroelastic approach using *Equivalent Static Loads (ESL)* for nonlinear static response matching was used in order to help capture structural nonlinearities. The main goal is to compare the results obtained with the same configuration of scaled model (*Configuration 2*) when classical (Method 2) and modern approach (ESL) are performed.

Nonlinear tip wing deflection obtained using the modern approach is compared to the target and traditionally designed model in *Figure 7.1a*. Tip wing deflection error is reduced to 14% and 11% at 4g for classical and modern approach, respectively. The trend of the tip wing deflection is considerably better when the scaled model is obtained using the modern approach.

Figure 7.1b and *7.1c* shows the *Fr-g* and *Fr-k* diagram for mode 4 and 7 when classical and modern approach are applied in order to match the aeroelastic response of the full model. In these figures it was decided to include only the fourth and the seventh mode because the flutter mode is due to a coupling of these two modes. The aeroelastic response is considerably more agreeable when the modern approach is applied in fact the accuracy is noticeably better than the results obtained for traditionally scaled models.

In the near future, the presented modifications (*ESL*) for the modern aeroelastic scaling approach should be tested for scaling aircraft with high aspect ratio wings.

In the longer term, the results obtained in this work should be applied to design experimental testing models that can demonstrate nonlinear geometric aeroelastic responses in flight. The scaled model should be tested in a wind tunnel for validating the applied methodology. The design methodology should be tested on higher fidelity computational models with more complex structural layouts (including for example composite materials, flight control surfaces, pylon modeled with a titanium alloy, a more accurate structural model in MSC Nastran™ software using solid elements, instead of just beam and shell elements, wing attachment should be also considered) and aerodynamic models of higher fidelity.

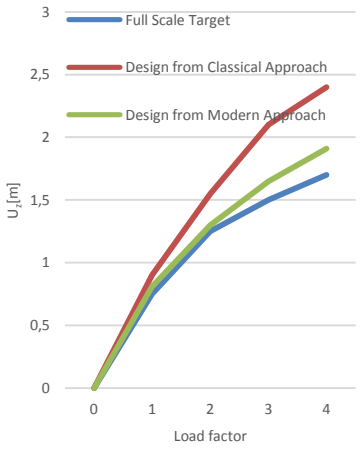

(a): Nonlinear tip deflection

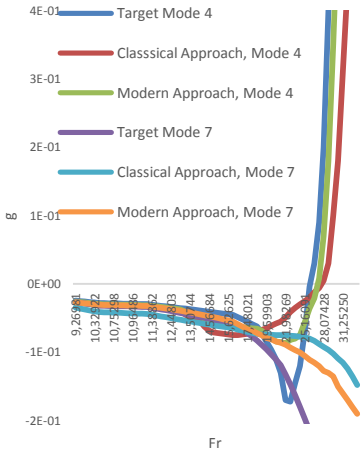

(b): Fr-g diagram

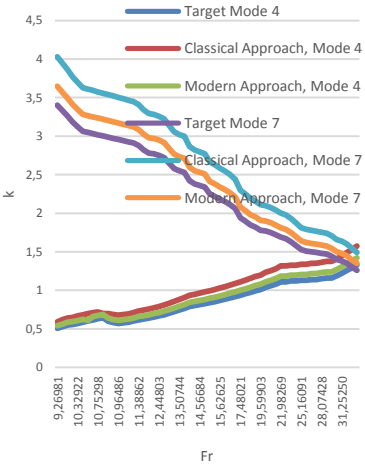

(c): Fr-k diagram

Figure 7.1: Nonlinear tip deflection, Fr-g and Fr-k diagram respectively

Bibliography

[1] Abbott, I., H. and Von Doenhoff, A. E., "Theory of Wing Sections, Including a Summary of Airfoil Data", Dover Pubblications, Inc., 1959

[2] Afonso, F., "Dynamic Scaling of a Joined Wing Aircraft Configuration", MSc Thesis, Universidade Técnica de Lisboa - Instituto Superior Técnico, July 2011

[3] Bisplinghoff, R. L., Ashley, H. and Halfman, R. L., "Aeroelasticity", Dover Pubblications, Addison-Wesley Publishing Company, Inc., New York, USA, 1996

[4] Cesnik, C. E. S., Patil, M. J. and Hodges, D. H., "Non Linear Aeroelasticity and Flight Dynamics of High-Altitude Long Endutrance Aircraft", AIAA Paper-99-1470, 1998

[5] Cooper, J. E. and Harmin, M. Y., "Dynamic Aeroelstic Prediction for Geometrically Nonlinear Arcraft", IFASD,2001.

[6] French, F. and Eastep, F. E., "Aeroelastic Model Sesign Using Parameter Identification", Journal of Aircraft, 33(1):198-202, 1996

[7] Galeán, O., "Optimization and Redesign of the Reaming Beam for Airbus A350 Pylons", Phd Thesis, Universidad Pontificia ICAI ICADE COMILLAS, Madrid, 2012

[8] Park, G. J., "Equivalent Static Loads Method for Nonlinear Static Response Structural Optimization", LS-DYNA Forum, Bamberg 2010

[9] Pereira, P., Almeida, L., Suleman, A., Bond, V., Canfield, R.A. and Blair, M., "Aeroelastic Scaling and Optimization of a Joined Wing Aircraft Concept", AIAA/ASME/ASCE/AHS/ASC Structures, Structural Dynamics and Materials Conference, 2007

[10] Pittit, C. L., Cranfield, R. A. and Ghanem, R., "Stochastic Analysis of a Aeroelastic System", New York : ASCE, 2002

[11 Ricciardi, P. A., "Geometrically Nonlinear Aeroelastic Scaling", Phd Dissertation, Faculty of the Virginia Polytechnic and State University, Blacksburg, Virginia, 2013

[12] Richards, J., "An Experimental Investigation of a Joined Wing Aircraft Configuration Using Flexible, Reduced Scale Flight Test Vehicles", Phd Dissertation, University of Victoria, Victoria, BC, Canada, 2014

[13] Richards, J. and Suleman, A., "Aeroelastic Scaling of Unconventional Joined Wing Concept for Exploration of Gust Load Response", IFASD-2009-177

[14] Spada, C., " Aeroelastic Analysis of High Aspect Ratio Wings", MSc Thesis, Universidade de Lisboa - Instituto Superior Técnico, 2014